Isolation of exosomes from whole blood by integrating acoustics and microfluidics

Mengxi Wu[a,b], Yingshi Ouyang[c], Zeyu Wang[a], Rui Zhang[b], Po-Hsun Huang[a], Chuyi Chen[a], Hui Li[c,d], Peng Li[e], David Quinn[f], Ming Dao[g,1], Subra Suresh[h,i,1], Yoel Sadovsky[c,i,1], and Tony Jun Huang[a,1]

[a]Department of Mechanical Engineering and Material Science, Duke University, Durham, NC 27708; [b]Department of Engineering Science and Mechanics, The Pennsylvania State University, University Park, PA 16802; [c]Department of Obstetrics, Gynecology, and Reproductive Sciences, Magee-Womens Research Institute, University of Pittsburgh, Pittsburgh, PA 15213; [d]The Third Xiangya Hospital, Central South University, Changsha, Hunan 410000, China; [e]Eugene Bennett Department of Chemistry, West Virginia University, Morgantown, WV 26506; [f]Department of Mechanical Engineering, Carnegie Mellon University, Pittsburgh, PA 15213; [g]Department of Materials Science and Engineering, Massachusetts Institute of Technology, Cambridge, MA 02139; [h]Nanyang Technological University, Singapore 639798; and [i]School of Medicine, University of Pittsburgh, Pittsburgh, PA 15261

Contributed by Subra Suresh, August 17, 2017 (sent for review June 5, 2017; reviewed by Gang Bao and M. Taher A. Saif)

Exosomes are nanoscale extracellular vesicles that play an important role in many biological processes, including intercellular communications, antigen presentation, and the transport of proteins, RNA, and other molecules. Recently there has been significant interest in exosome-related fundamental research, seeking new exosome-based biomarkers for health monitoring and disease diagnoses. Here, we report a separation method based on acoustofluidics (i.e., the integration of acoustics and microfluidics) to isolate exosomes directly from whole blood in a label-free and contact-free manner. This acoustofluidic platform consists of two modules: a microscale cell-removal module that first removes larger blood components, followed by extracellular vesicle subgroup separation in the exosome-isolation module. In the cell-removal module, we demonstrate the isolation of 110-nm particles from a mixture of micro- and nanosized particles with a yield greater than 99%. In the exosome-isolation module, we isolate exosomes from an extracellular vesicle mixture with a purity of 98.4%. Integrating the two acoustofluidic modules onto a single chip, we isolated exosomes from whole blood with a blood cell removal rate of over 99.999%. With its ability to perform rapid, biocompatible, label-free, contact-free, and continuous-flow exosome isolation, the integrated acoustofluidic device offers a unique approach to investigate the role of exosomes in the onset and progression of human diseases with potential applications in health monitoring, medical diagnosis, targeted drug delivery, and personalized medicine.

extracellular vesicles | exosomes | blood-borne vesicles | surface acoustic waves | acoustic tweezers

Exosomes are cell-derived nanovesicles (1), ≈30–150 nm in diameter, that carry nucleic acids, proteins, lipids, and other molecules from their cells of origin (2, 3). Exosomes transfer RNA and proteins to the cells they fuse with and play important roles in cell-to-cell communication. Recent research into the characteristics and mechanisms involving exosomes has introduced the potential development of biomarkers for health monitoring and diagnosis of a number of human diseases, including cancer (4), neurodegenerative disease (5), and diseases of the kidney (6), liver (7), and placenta (8). Exosomes represent a unique research opportunity because they are found in nearly all biological fluids (9–11), including blood, saliva, urine, semen, sputum, breast milk, and cerebrospinal fluid. Unlike tissue samples, they can be collected noninvasively over a long period, allowing for continuous monitoring of disease progression and response to therapy. Exosomes also have several advantages over other circulating biomarkers. They are abundant (thousands to billions per microliter of biofluid), and their durability suggests that their internal integrity can be preserved through several freeze-and-thaw cycles.

Currently, differential centrifugation (including gradient ultracentrifugation), which relies on multiple centrifugation steps to sequentially remove whole cells, cellular debris, and subgroups of extracellular vesicles (EVs) based on their different sizes and densities, is a standard technology for isolating exosomes (12, 13). While differential centrifugation achieves high purity, it is time-consuming (several hours to days), expensive, and inefficient (in that the exosome isolation yields from whole blood are typically low, 5–40% of preseparation exosome population) (12, 14–17). It also requires trained personnel to operate. Moreover, the high centrifugal force used in ultracentrifugation (100,000–200,000 × g) has been shown to cause exosome fusion, promote coagulation, and alter their structures, properties, and functions, which may impact downstream analysis (12, 13, 18). Other methods, including immunoaffinity capture (19, 20), precipitation kits such as ExoQuick (System Biosciences) and Total Exosome Isolation (Invitrogen) (12, 21), microfluidics (17, 22, 23), nanoscale lateral displacement arrays (24), nanostructure-based filtration (25), nanoplasmonic chip (26), magnetoelectrochemical sensor (27), and dialysis membrane filtration (28), have been implemented. However, these methods frequently suffer from drawbacks such as the need for additional reagents/labels, long processing time, low reproducibility, low exosome integrity, low exosome purity, and/or low exosome yield.

Acoustic waves are well-recognized for their high precision and biocompatibility in manipulating cells and other bioparticles

Significance

We have developed a unique, integrated, on-chip technology that is capable of isolating exosomes or other types of extracellular vesicles, directly from undiluted whole-blood samples in an automated fashion. Automated exosome isolation enables biohazard containment, short processing time, reproducible results with little human intervention, and convenient integration with downstream exosome analysis units. Our method of integrating acoustics and microfluidics leads to the isolation of exosomes with high purity and yield. With its label-free, contact-free, and biocompatible nature, it offers the potential to preserve the structures, characteristics, and functions of isolated exosomes. This automated, point-of-care device can further help in advancing exosome-related biomedical research with potential applications in health monitoring, disease diagnostics, and therapeutics.

Author contributions: M.W., Y.O., S.S., Y.S., and T.J.H. designed research; M.W., Y.O., Z.W., R.Z., C.C., and H.L. performed research; M.W., Y.O., Y.S., and T.J.H. contributed new reagents/analytic tools; M.W., Y.O., P.-H.H., P.L., D.Q., M.D., S.S., Y.S., and T.J.H. analyzed data; and M.W., Y.O., P.-H.H., P.L., D.Q., M.D., S.S., Y.S., and T.J.H. wrote the paper.

Reviewers: G.B., Rice University; and M.T.A.S., University of Illinois at Urbana–Champaign.

The authors declare no conflict of interest.

Freely available online through the PNAS open access option.

[1]To whom correspondence may be addressed. Email: mingdao@mit.edu, ssuresh@ntu.edu.sg, ysadovsky@mwri.magee.edu, or tony.huang@duke.edu.

This article contains supporting information online at www.pnas.org/lookup/suppl/doi:10.1073/pnas.1709210114/-/DCSupplemental.

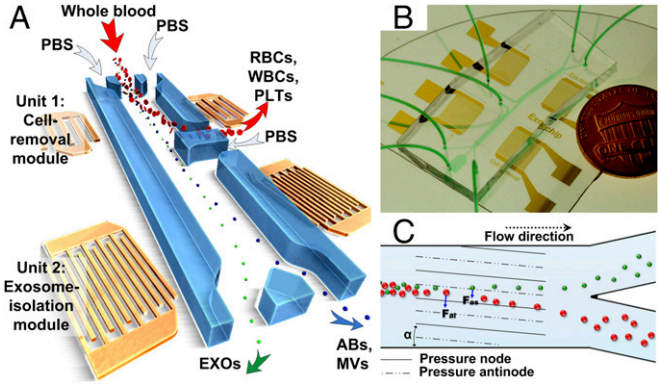

Fig. 1. Schematic illustration and mechanisms underlying integrated acoustofluidic device for isolating exosomes. (*A*) RBCs, WBCs, and PLTs are filtered by the cell-removal module, and then subgroups of EVs (ABs: apoptotic bodies; EXOs: exosomes; MVs: microvesicles) are separated by the exosome-isolation module. (*B*) An optical image of the integrated acoustofluidic device. Two modules are integrated on a single chip. (*C*) Size-based separation occurs in each module due to the lateral deflection induced by a taSSAW) field. The periodic distribution of pressure nodes and antinodes generates an acoustic radiation force to push large particles toward node planes.

(29–34). Current acoustic-based separation strategies, however, can only handle biological fluids (such as undiluted blood), which must be preprocessed before exosome separation, and thus require additional equipment and time, and are subject to the risk of sample loss. Additionally, current acoustic separation strategies can only differentiate two types of targets, making it difficult to isolate exosomes directly from complex multicomponent fluids such as undiluted blood.

Here, we demonstrate an acoustofluidic platform (i.e., one that involves the fusion of acoustics and microfluidics) which can isolate exosomes directly from undiluted blood samples. This acoustofluidics-based, automated point-of-care system allows single-step, on-chip isolation of exosomes from biological fluids (such as blood, urine, saliva, plasma, and breast milk) or in vitro cell cultures. It also represents a unique integration of two sequential surface acoustic wave (SAW) microfluidic modules, comprising a cell-removal module and an exosome-isolation module. Each module relies on a tilted-angle standing SAW (taSSAW) field (29, 30) formed by one pair of interdigital transducers (IDTs). The cell-removal module first extracts microscale blood components to obtain enriched EVs, while the exosome-isolation module further purifies the exosomes by removing the other EV subgroups. After optimizing the length, driving frequency, and driving power of the IDTs in the two modules, we successfully isolated exosomes from undiluted blood samples with high purity and yield. Compared with existing methods, our acoustofluidic platform provides a simple, rapid, efficient, and potentially cost-effective and biocompatible strategy.

Theory and Mechanism

Fig. 1 *A* and *B* presents a schematic view and a photograph of our acoustofluidic platform, which includes a cell-removal module and an exosome-isolation module arranged in series. The cell-removal module is designed first to fractionate blood components larger than 1 μm in diameter, including red blood cells (RBCs), white blood cells (WBCs), and platelets (PLTs). This provides cell-free plasma for downstream exosome isolation, which is optimized to separate nanoscale bioparticles. By using a higher frequency (~40 MHz) than those used in our previous acoustofluidic devices designed for cell separation (30), the exosome-isolation module is capable of discriminating submicrometer particles, such that subgroups of EVs with larger size (including microvesicles and apoptotic bodies), from exosomes. Fig. 1*C* illustrates the mechanism for separating large particles from small ones due to the deflection caused by acoustic pressure nodes tilted with respect to the channel orientation. Particles are subjected to an acoustic radiation force (F_r) generated by the SAW field, and are pushed toward the pressure node. As particles move toward the pressure nodes, their movement is impeded by the Stokes drag force (F_d). The drag force is proportional to the radius of particles or cells and the acoustic radiation force is proportional to the volume. Thus, the acoustic radiation force dominates over the drag force for larger particles, which causes the particle stream to migrate toward the tilted nodes. Conversely, the drag force cancels a significant part of acoustic radiation force out for smaller particles, resulting in little lateral displacement. By adjusting the input power, the cutoff particle diameter can be adjusted, giving our device the flexibility to be used in a wide variety of applications. More details can be found in *SI Theory and Mechanism*.

Results

Cell-Removal Module. To optimize parameters for the cell-removal module, we first examined whether our method could separate mixtures of synthetic particles of two different sizes using a standalone cell-removal module. We first mixed polystyrene particles of diameter 970 nm (representative of larger-diameter EVs in human blood) and 5.84 μm (representative of blood cells such as RBCs and WBCs). The 970-nm particles were conjugated with a green fluorophore, facilitating real-time tracking of their trajectory during the course of separation. We forced the particle mixture into a narrow, straight sample stream by introducing two PBS sheath flows through two adjacent inlets. Using an applied voltage of 22 Vpp (peak-to-peak voltage) and driving frequency of 19.6 MHz, we were able to direct the 5.84-μm-diameter particles toward the waste outlet, whereas the 970-nm-diameter particles remained in the sample stream and exited through the collection outlet (Fig. 2). We then repeated this experiment, replacing the 970-nm particles with 110-nm polystyrene particles, which better represent exosomes. Using the same cell-removal module, we could separate polystyrene particles of 110 nm from particles of 5 μm, with a recovery rate of over 99% (Fig. S1). These results demonstrate the capability of

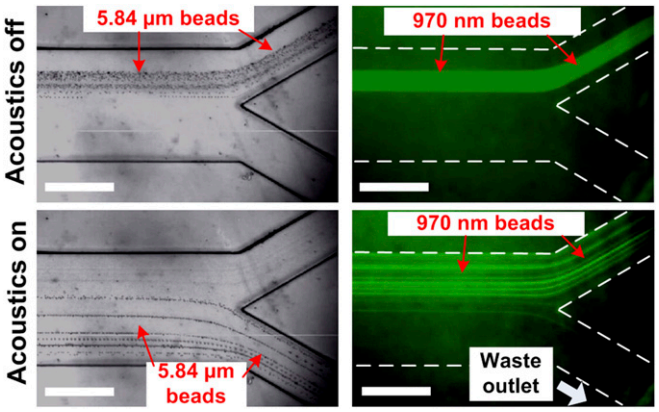

Fig. 2. Separation of synthetic microparticles and submicrometer particles using the acoustofluidic cell-removal module. Polystyrene particles with diameters of 5.84 μm (not labeled) and 970 nm (labeled with Dragon Green fluorescent dye) were processed through the acoustic field. The taSSAW field deflected microparticles to the waste outlets. The acoustic radiation force was not sufficiently large to move the submicrometer particles, which were therefore separated from microparticles at the outlet. White stripe in the two left panels indicates the centerline location of the CCD (charge-coupled device) image sensor. (Scale bar: 500 μm.)

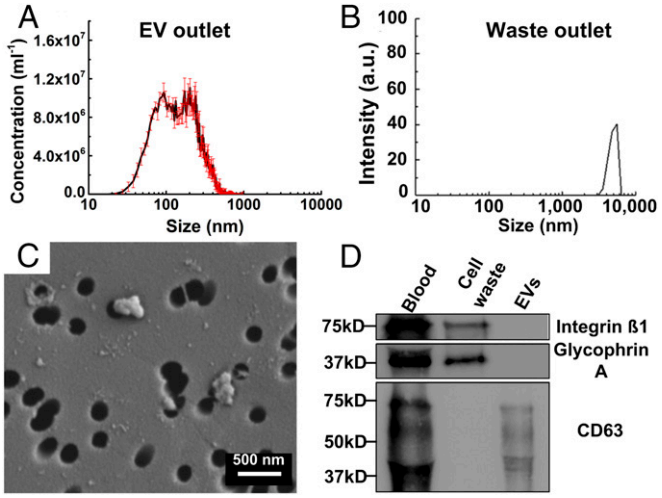

Fig. 3. Characterization of the cell-removal module. (*A*) Separation of EVs from RBCs and other blood components. NTA was used to characterize the isolated EVs from the collection outlet. (*B*) RBCs and other blood components collected from waste outlet were characterized by DLS. The ordinate is the relative intensity of signals measured. (*C*) SEM image of isolated EVs sample loaded on a filter membrane. The EV sample contained vesicles of diameters from ~50 to 300 nm. (*D*) Western blot with expression of RBC marker (GYPA), PLT marker (integrin β1), and EV markers (CD63). The proteins from blood, cell waste sample, and isolated EVs were extracted and prepared for electrophoresis.

this acoustofluidic approach to isolate nanoparticles from a mixture of nanoparticles and microparticles.

Based on the conditions optimized by our particle-separation experiments, we proceeded to test our cell-removal module using undiluted whole-blood samples, which contained the anticoagulant EDTA. Because blood cells have a lower acoustic contrast than polystyrene particles, we increased the applied voltage to 40 Vpp. To match the acoustic impedance of whole blood, a 5% dextrose solution in PBS was used as sheath fluid. When the taSSAW field was off, the whole-blood sample flowed into the top outlet. Once the taSSAW was activated, blood components such as RBCs, WBCs, and PLTs changed their flow route and were delivered to the waste outlet (Fig. S2 *A* and *B*) and the smaller EV-containing sample was collected.

Samples collected from the two outlets were measured using nanoparticle tracking analysis (NTA) device and dynamic light scattering (DLS). The sample collected at the waste outlet had a visible peak at ~5 μm, which contained primarily RBCs, while the sample collected at the collection outlet, the isolated EVs sample, contained no particles larger than 1 μm (Fig. 3 *A* and *B*), thus suggesting that submicrometer particles, such as EVs, were isolated. We used a scanning electron microscope (SEM) and Western blotting to further characterize isolated EVs. The SEM showed that the diameter of isolated EVs ranged between 50 and 300 nm (Fig. 3*C*). The Western immunoblotting showed that samples from the waste outlet were positive for Integrin β1 (PLT marker) and Glycophrin A (a representative marker of RBCs). In contrast, our isolated EVs were immune-positive for CD63, a tetraspanin characteristic of exosomal marker, and negative for PLT and RBC markers (Fig. 3*D*). Collectively, these results demonstrate that the acoustofluidic cell-removal module is capable of separating EVs directly from undiluted, anticoagulated human blood samples.

Exosome-Isolation Module. To examine whether our exosome-isolation module could separate EV subgroups, namely microvesicles from exosomes, we input a mixture of purified exosomes and microvesicles derived from primary human trophoblasts (PHTs) to a standalone exosome-isolation module. The isolation and culture of PHT cells from human placentas and the purification of PHT-derived microvesicles and exosomes from PHT-conditioned medium were described elsewhere (16). We identified an optimized driving frequency of 39.4 MHz based on pilot experiments using a nanoparticle mixture of 110 and 340 nm (Fig. S3). Then, we set the sample flow rate and sheath flow rate as 4 and 8 μL/min, respectively. With the standing SAW field switched on, and under an input voltage of 45 Vpp, larger bioparticles were deflected and directed to the waste outlet. We then conducted NTA of the isolated samples from both outlets as well as of the original mixture of the same volume. The original mixture of purified microvesicles and exosomes exhibited a broad size distribution from ~50 to 600 nm (Fig. 4*A*); specifically, there was a single peak at 122 nm corresponding to exosomes, whereas other peaks appeared between 170 and 300 nm, representing the broader distribution of microvesicles rather than exosomes. Additionally, the concentration distribution curve reached a valley at 140 nm, which was therefore chosen as the separation cutoff size. The sample at the collection outlet exhibited two peaks, at ≈81 and 99 nm, which represented slight shifts from the inlet peak corresponding to a size of 122 nm. This difference may be attributed to the resolution limits of NTA when testing highly heterogeneous samples. When we examined the morphology of the isolated exosomes (Fig. 4*C*) using transmission electron microscopy (TEM), the mean size of isolated vesicles was ~100 nm, which is consistent with the NTA results and the predicted size of exosomes. In contrast, the sample collected from the waste outlet exhibited several peaks larger than 170 nm, along with very few components that were less than 100 nm. These results demonstrated that our acoustofluidic device was able to separate two distinct EVs from each other (i.e., PHT-derived microvesicles from exosomes).

We further used NTA to quantify the concentrations of the mixture of trophoblastic microvesicles and exosomes, isolated microvesicles, and isolated exosomes. Given that the final

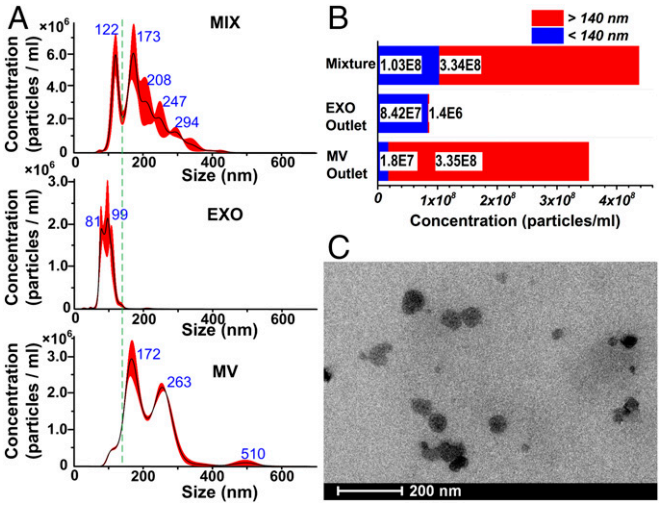

Fig. 4. Separation of exosomes from microvesicles using the exosome-isolation module. (*A*) Size distribution of original mixture (MIX), isolated EXO, and MV samples. The data were obtained from at least three NTA assays. The black line and the red area represent the fitting curve and the error bar, respectively. The *y* axis is the concentration of particles. The peak positions are marked. The green dashed line is located at 140 nm, which is set as the cutoff size. (*B*) Quantitative characterization of exosome/microvesicle separation, showing the concentrations of vesicle subgroups (cutoff size at 140 nm) in the mixture and processed samples. The concentration is expressed as the number of particles per microliter. (*C*) TEM image of isolated exosome samples.

volume of each outlet is 1.5× the input sample volume, reflecting the PBS dilution effect during the course of separation, we corrected the particle concentrations measured from NTA by dividing by this dilution factor (1.5). We calculated that the original mixture contained 1.03×10^8 particles per microliter that were smaller than 140 nm and 3.34×10^8 particles per microliter that were larger than 140 nm. The concentration of particles collected from the exosome outlet was 8.42×10^7 per microliter (<140 nm) and 1.4×10^6 per microliter (>140 nm). At the microvesicle outlet, the particle concentration was 1.8×10^7 per microliter (<140 nm) and 3.35×10^8 per microliter (>140 nm). The total numbers of vesicles before and after separation were 4.37×10^8 per microliter and 4.386×10^8 per microliter, respectively, and the percentages of small (<140 nm) particles were comparable before (23.6%) and after (23.3%) separation. These values suggest that the acoustofluidics-based separation technique had a high sample yield with minimal loss during the separation process. We defined the recovery rate as the fraction of particles recovered below 140 nm among the particles of that size in the inlet solution. Similarly, we define the purity of particle isolation as the fraction of isolated particles below 140 nm among the collected particles of all sizes. Overall, the present exosome-isolation device showed a recovery rate and purity of 82.4% and 98.4%, respectively, for particles smaller than 140 nm in diameter. Despite the demonstrated recovery rate and purity, it should be noted that the particles smaller than 140 nm may contain nonexosomal particles and protein aggregates, which could be considered contaminants for downstream analysis of exosome.

Isolation of Exosomes from Undiluted Blood Using the Integrated Device. Following testing and optimizing the individual modules, we integrated the cell-removal module and exosome-isolation module into a single acoustofluidic chip. On this integrated chip, the distance between the two modules was set sufficiently apart to avoid interference between the acoustic fields of the two modules, allowing the integrated device to operate as efficiently as the optimized individual modules using the same parameters and designs. We used undiluted human blood from healthy donors for EV isolation (Fig. 5 and Fig. S4). The flow rates of each inlet were set to 4 μL/min for the blood sample, 4 and 12 μL/min for sheath flows in the cell-removal module, and 10 μL/min for sheath flow in the exosome-isolation module. The driving frequency and voltage of the input rf signal for the integrated device were the same as those used for individual modules described above. When the acoustic field was off, the blood stream was focused in the middle of channel and directed into the device outlet F in Fig. 5 (*Top Left*). When the rf signal was on for both modules, blood components were separated into different outlets after passing through the cell-removal module. The vast majority of blood cells and PLTs were deflected to a cell waste outlet (outlet D in Fig. 5, *Top Left*) and the remaining components continued to flow downstream to the exosome-isolation module where the apoptotic bodies, microvesicles, and the remaining part of cells are deflected to the vesicle waste outlet (G in Fig. 5, *Top Left*), thereby isolating exosomes from whole-blood samples in the device outlet (F in Fig. 5, *Top Left*), which we subsequently refer to as the "exosome outlet."

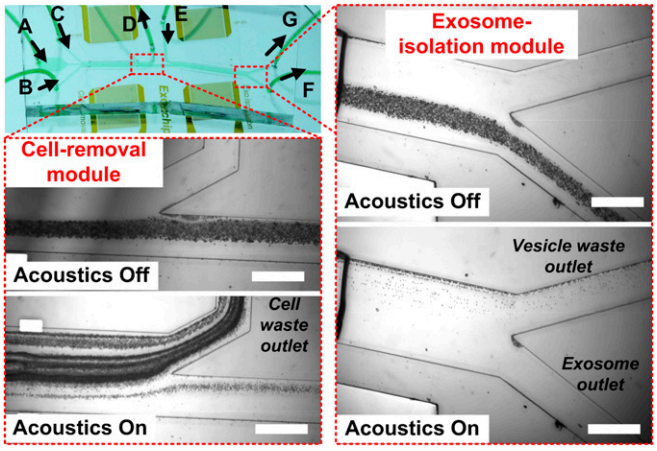

Fig. 5. Isolation of exosomes from whole blood using the integrated device using acoustofluidics. In our experiments, inlet A is for whole blood; inlets B, C, and E are for sheath flows. Outlet D is cell waste. Outlets F and G are for isolated exosomes and vesicle waste, respectively. Images were taken under the microscope at the corresponding areas of the device. Blood components were directed to each corresponding outlet when the acoustic wave was on. White stripe in the four grayscale panels indicates the centerline location of the CCD image sensor. (Scale bar: 500 μm.)

Upon collecting samples from the exosome and vesicle waste outlets, we characterized the cell-removal efficiency. The original blood sample, separated vesicle waste, and isolated exosome sample were each collected into 1.5-mL centrifuge tubes and spun at 3,000 rpm for 10 min. As shown in Fig. 6*A*, the volume of cells in the whole-blood sample was nearly half of the total volume, which is typical for human blood. In contrast, there were few (<0.1%) blood cells remaining in the isolated exosome sample and the vesicle waste (Fig. 6*A*). We further quantified the number of blood cells in the exosome sample, using a hemocytometer. The concentration of cells was 2.08×10^4 per milliliters in the sample collected from the exosome outlet, while the RBC count reference ranged from 4.7 to 6.1×10^{10} per milliliter, yielding a cell-removal rate greater than 99.999%. We then measured the size distribution of isolated exosome samples through NTA. This was compared with NTA of plasma that was separated from the whole-blood sample using standard centrifugation. The sample collected from the exosome outlet showed a clear, narrow peak at around 100 nm, which corresponded to exosomes, while the plasma control displayed a flat, disperse curve covering a broad range from ∼50 nm to 1 μm (Fig. 6*B*). As control, we isolated human plasma exosomes using OptiPrep gradient ultracentrifugation, and compared the size distribution of exosomes isolated by two different approaches. The peak of exosomes using gradient ultracentrifugation was slightly larger than that of exosomes using the acoustofluidic device (Fig. S5). This difference could be explained by the effect of ultracentrifugation on exosomes, causing some aggregation of exosomes and/or even fusion of small, "contaminating" particles (18, 35). Collectively, the NTA results demonstrated that the acoustofluidic device differentiated subgroups of EVs based on size, and thereby isolated exosomes from the mixture.

Having demonstrated the removal of blood components, including RBCs, WBCs, PLTs, and microvesicles from undiluted whole-blood samples, we sought to verify that the sample isolated from blood is indeed composed of exosomes. We used Western blot analysis to examine the expression of exosomal protein markers in the samples collected from all three outlets and a diluted blood sample. We analyzed the expression of EV membrane tetraspanin CD63, membrane-binding protein TSG101, endoplasmic reticulum protein HSP90, and heat shock cognate protein 70 (HSC70). Among the four samples examined, the sample collected from the exosome outlet showed a high expression of HSP90, HSC70, CD63, and TSG101 (Fig. 6*C*), confirming the presence of exosomes in the samples. These proteins were also present in original blood samples, as expected. The other two outlets, referred to as vesicle waste and cell waste, showed very low levels of exosomal markers.

We further investigated whether exosomes isolated by our integrated acoustofluidic chip were contaminated by RBC's RNA transcripts. It has been demonstrated (36) that four mRNA genes encoding Ferritin light chain (FTL), Glycophorin A (GYPA),

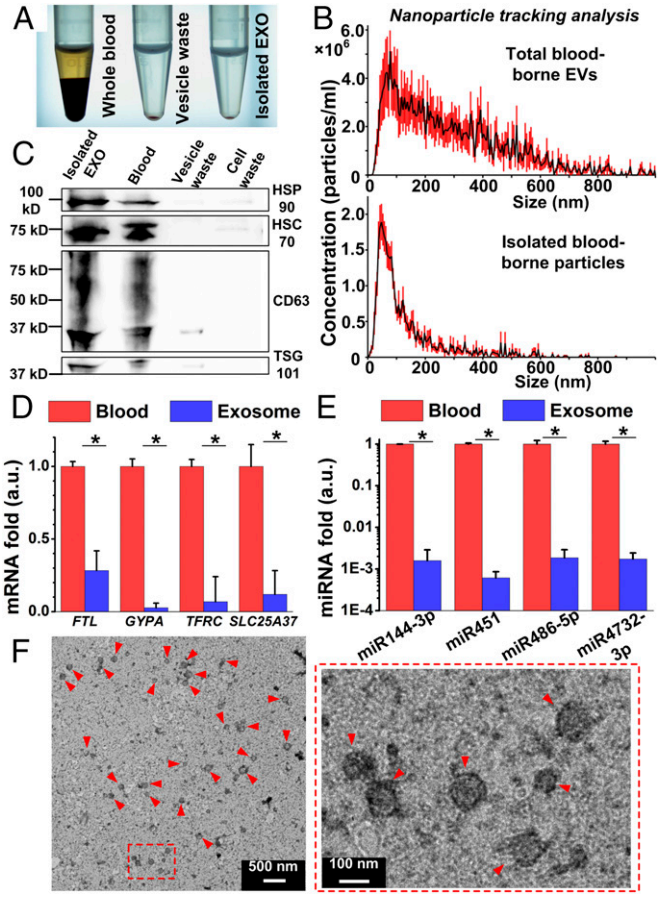

Fig. 6. Characterization of exosome isolation from whole blood using the integrated acoustofluidic chip. (*A*) Removal of blood cells and PLTs. In the original sample (undiluted whole blood), RBCs occupied approximately half of the volume. The isolated exosome sample and vesicle waste sample contain a minimal amount of blood cells. (*B*) EVs in blood plasma showed a dispersed size distribution that ranged between 30 nm and 1 μm. The size distribution of collected exosome sample exhibited a major peak at <100 nm. (*C*) Western blot of exosome markers, showing a prominent expression in the isolated exosome and blood samples, while the other samples (vesicle waste and cell waste) exhibited low expression level of exosomal proteins. (*D* and *E*) The expression (expressed as relative fold difference) of individual mRNAs (*D*) and miRNAs (*E*) in human blood and isolated exosomes. The data represent three independent experiments. *$P < 0.05$ (ANOVA) (*F*) TEM images of isolated exosomes. The exosomes (red arrows) have a characteristic round shape and a cup-like structure.

Transferrin receptor (TFRC), and Solute carrier family 25 member 37 (SLC25A37) are predominantly expressed in human RBCs. We compared the relative levels of these transcripts in samples of human blood input and isolated exosomes. We found that all four transcripts expressed in RBCs were decreased by 75∼90% between the input to the first module and the output from the second module in our acoustofluidic device (Fig. 6*D*). Similarly, we examined relative levels of RBC-dominant miRNAs in whole blood and isolated exosomes. miRNAs are known to be packaged in exosomes and other extracellular vesicles, and RBCs strongly express four miRNAs including miR-144–3p, miR-451, miR-486–5p, and miR-4732–3p (37–40). Consistent with the mRNA results (Fig. 6*D*), our miRNA results (Fig. 6*E*) indicated that isolated exosomes barely, if any, expressed these four RBC miRNAs. We observed a similar pattern of mRNA and miRNA expression using samples derived from the gradient-based ultracentrifugation (Fig. S6). Together, the mRNA and miRNA results suggest that the exosomes isolated by our acoustofluidic devices have little contamination by RBCs. Finally, we examined the morphology of isolated exosomes using TEM. A large number of vesicles were, as marked by arrows, of diameter ∼100 nm with cup-like concavity (Fig. 6*F*), consistent with the established morphology of exosomes (41). These results support the ability of our acoustofluidic platform to isolate morphologically intact exosomes.

Discussion

We have demonstrated an acoustofluidic platform that is capable of isolating exosomes directly from undiluted human blood. The integrated device is based on acoustofluidics and contains two separation modules, which provide the flexibility to handle multiple subpopulations of a complex sample. By tuning the input power of the rf signal and fluid flow rates, the cutoff size for each of the two separation modules can be adjusted to ensure the selection of specific subgroups. This feature enables the flexibility to adjust for a range of particle sizes and applications.

Blood is one of the most complex biological fluids, with components and properties that vary greatly among individuals or within an individual at different time points. These factors challenge existing separation techniques. Consider, for example, the experimental hurdles arising from the blood lipid level. The lipid particles have a negative acoustic contrast, in that they are pushed to antinodes in the standing acoustic field. As such, lipid particles concentrate at antinodes and tend to aggregate (36). Aggregation of lipids disturbs laminar flow and the acoustic field pattern, which in turn reduces separation efficiency. Therefore, for blood samples with high lipid levels, the sheath/sample flow ratio needs to be appropriately adjusted with an increased buffer flow rate to suppress lipid aggregation. Another solution might be the addition of a third acoustofluidic module designed to remove lipids from undiluted blood.

With the current device configuration, we have successfully separated and isolated bioparticles larger than 150 nm from exosomes. Notably, this isolated exosome sample may contain nonexosomal particles and protein aggregates that have a size similar to exosomes or smaller particles. To obtain exosomes with the highest purity, we plan to integrate additional acoustofluidic-based separation modules into the current device setup. As indicated in Table S1, Fig. S7, and *SI Simulation Assays for Isolating Nonexosomal Particles and Soluble Proteins from Exosomes*, these additional acoustofluidic modules will allow us to further isolate exosomes from (*i*) particles that have a similar size to exosomes (30–150 nm) but different acoustic contract factors, and (*ii*) particles that are smaller (i.e., <30 nm) than exosomes.

Our technology, predicated upon acoustofluidics, offers the following distinct advantages over other available means to separate exosomes from biological fluids:

i) Automation, high reproducibility, and biohazard containment: In conventional exosome-isolation assays, samples need to be subjected to a multistep protocol using several instruments. Throughout this process, a trained technician must manually interact with the samples. In contrast, the acoustofluidic approach can isolate exosomes (or other subgroups of EVs) directly from biological fluids (e.g., undiluted blood) with a single device in an automated manner. Thus, it offers a simpler approach with enhanced biosafety and a higher likelihood of consistent and reliable results. Furthermore, after determining the optimal acoustic field settings, routine operation of the acoustofluidic system requires less training compared with conventional approaches.

ii) Exosome-separation speed: While differential centrifugation approaches take hours to days for exosome isolation from whole blood, the entire process to isolate exosomes from 100 μL undiluted human blood can be achieved within ∼25 min using acoustofluidics.

iii) Exosome yield and purity: We have demonstrated an exosome purity of ∼98% and a yield of ∼82% by using a mixture

of purified exosomes and microvesicles derived from PHT cells in our experiments.

iv) Continuous flow configuration: Many exosome-separation platforms must be operated in batch mode. Acoustofluidics is capable of separating exosomes in continuous flow. Such devices involving continuous flow can be conveniently integrated into existing microfluidic-based exosome analysis device to enable an all-in-one, on-chip exosome processing and analysis system.

v) Potential to isolate structurally intact and biologically active exosomes: Many existing exosome-isolation technologies have difficulties in isolating biologically active and structurally intact exosomes; the isolation process often alters the morphology, content, and functions of the exosomes (14, 18, 42). The present strategy offers a label-free, contact-free, and potentially gentle method that has the potential to minimize disruption of the captured exosomes. The acoustic power intensity and frequency we used in our experiments are in a similar range to those in ultrasonic imaging, which has been proven to be a safe technique. Using our device, exosomes are exposed to a low-power-intensity acoustic field for several seconds. This may compare favorably to differential centrifugation, which subjects exosomes to hours of exposure to forces as high as 200,000 × *g*. This combination of factors yields a higher likelihood of preserving the biological, biophysical, and structural integrity of the isolated exosomes for further investigation.

Methods

Device Fabrication and Experimental Setup. The device is fabricated by standard soft-lithography and lift-off process. More details are in *SI Device Fabrication* and *SI Experimental Setup*.

Isolation of Exosomes Using Gradient Ultracentrifugation. Exosomes were isolated from whole-blood specimens using an OptiPrep gradient ultracentrifugation as previously described (16). The collection of placentas used for cell isolation and culture was reviewed and approved by the Institutional Review Board (IRB) at the University of Pittsburgh.

Characterization of Exosomes. The isolated exosomes are characterized by NTA, Western blot, electron microscopy, and quantitative polymerase chain reaction (qPCR). More details can be found in *SI Characterization of Exosomes*.

ACKNOWLEDGMENTS. The authors are grateful to Hunter Bachman for editing the manuscript. We acknowledge support from the National Institutes of Health (Grant R01 HD086325) and National Science Foundation (Grant IIP-1534645). M.D. acknowledges partial support from Singapore - Massachusetts Institute of Technology Alliance for Research and Technology (SMART).

1. Sokolova V, et al. (2011) Characterisation of exosomes derived from human cells by nanoparticle tracking analysis and scanning electron microscopy. *Colloids Surf B Biointerfaces* 87:146–150.
2. Valadi H, et al. (2007) Exosome-mediated transfer of mRNAs and microRNAs is a novel mechanism of genetic exchange between cells. *Nat Cell Biol* 9:654–659.
3. Anand PK (2010) Exosomal membrane molecules are potent immune response modulators. *Commun Integr Biol* 3:405–408.
4. Thind A, Wilson C (2016) Exosomal miRNAs as cancer biomarkers and therapeutic targets. *J Extracell Vesicles* 5:31292.
5. Russo I, Bubacco L, Greggio E (2012) Exosomes-associated neurodegeneration and progression of Parkinson's disease. *Am J Neurodegener Dis* 1:217–225.
6. Miranda KC, et al. (2010) Nucleic acids within urinary exosomes/microvesicles are potential biomarkers for renal disease. *Kidney Int* 78:191–199.
7. Bala S, et al. (2012) Circulating microRNAs in exosomes indicate hepatocyte injury and inflammation in alcoholic, drug-induced, and inflammatory liver diseases. *Hepatology* 56:1946–1957.
8. Delorme-Axford E, et al. (2013) Human placental trophoblasts confer viral resistance to recipient cells. *Proc Natl Acad Sci USA* 110:12048–12053.
9. Gonzales PA, et al. (2009) Large-scale proteomics and phosphoproteomics of urinary exosomes. *J Am Soc Nephrol* 20:363–379.
10. Lässer C, et al. (2011) Human saliva, plasma and breast milk exosomes contain RNA: uptake by macrophages. *J Transl Med* 9:9.
11. Poliakov A, Spilman M, Dokland T, Amling CL, Mobley JA (2009) Structural heterogeneity and protein composition of exosome-like vesicles (prostasomes) in human semen. *Prostate* 69:159–167.
12. Van Deun J, et al. (2014) The impact of disparate isolation methods for extracellular vesicles on downstream RNA profiling. *J Extracell Vesicles* 3:24858.
13. Yang F, Liao X, Tian Y, Li G (2017) Exosome separation using microfluidic systems: Size-based, immunoaffinity-based and dynamic methodologies. *Biotechnol J* 12:1600699.
14. Lamparski HG, et al. (2002) Production and characterization of clinical grade exosomes derived from dendritic cells. *J Immunol Methods* 270:211–226.
15. Greening DW, Xu R., Ji H, Tauro BJ, Simpson RJ (2015) A protocol for exosome isolation and characterization: Evaluation of ultracentrifugation, density-gradient separation, and immunoaffinity capture methods. *Proteomic Profiling: Methods and Protocols*, ed. Posch A (Springer New York), pp. 179–209.
16. Ouyang Y, et al. (2016) Isolation of human trophoblastic extracellular vesicles and characterization of their cargo and antiviral activity. *Placenta* 47:86–95.
17. Liga A, Vliegenthart AD, Oosthuyzen W, Dear JW, Kersaudy-Kerhoas M (2015) Exosome isolation: A microfluidic road-map. *Lab Chip* 15:2388–2394.
18. Linares R, Tan S, Gounou C, Arraud N, Brisson AR (2015) High-speed centrifugation induces aggregation of extracellular vesicles. *J Extracell Vesicles* 4:29509.
19. Mathivanan S, et al. (2010) Proteomics analysis of A33 immunoaffinity-purified exosomes released from the human colon tumor cell line LIM1215 reveals a tissue-specific protein signature. *Mol Cell Proteomics* 9:197–208.
20. Jørgensen M, et al. (2013) Extracellular vesicle (EV) array: Microarray capturing of exosomes and other extracellular vesicles for multiplexed phenotyping. *J Extracell Vesicles* 2:20920.
21. Zeringer E, Barta T, Li M, Vlassov AV (2015) Strategies for isolation of exosomes. *Cold Spring Harb Prot* 2015:319–323.
22. Chen C, et al. (2010) Microfluidic isolation and transcriptome analysis of serum microvesicles. *Lab Chip* 10:505–511.
23. Kanwar SS, Dunlay CJ, Simeone DM, Nagrath S (2014) Microfluidic device (ExoChip) for on-chip isolation, quantification and characterization of circulating exosomes. *Lab Chip* 14:1891–1900.
24. Wunsch BH, et al. (2016) Nanoscale lateral displacement arrays for the separation of exosomes and colloids down to 20 nm. *Nat Nanotechnol* 11:936–940.
25. Wang Z, et al. (2013) Ciliated micropillars for the microfluidic-based isolation of nanoscale lipid vesicles. *Lab Chip* 13:2879–2882.
26. Im H, et al. (2014) Label-free detection and molecular profiling of exosomes with a nano-plasmonic sensor. *Nat Biotechnol* 32:490–495.
27. Jeong S, et al. (2016) Integrated magneto-electrochemical sensor for exosome analysis. *ACS Nano* 10:1802–1809.
28. Cho S, et al. (2016) Isolation of extracellular vesicle from blood plasma using electrophoretic migration through porous membrane. *Sens Actuators B Chem* 233:289–297.
29. Ding X, et al. (2014) Cell separation using tilted-angle standing surface acoustic waves. *Proc Natl Acad Sci USA* 111:12992–12997.
30. Li P, et al. (2015) Acoustic separation of circulating tumor cells. *Proc Natl Acad Sci USA* 112:4970–4975.
31. Li S, et al. (2016) Acoustofluidic transfer of inflammatory cells from human sputum samples. *Anal Chem* 88:5655–5661.
32. Laurell T, Petersson F, Nilsson A (2007) Chip integrated strategies for acoustic separation and manipulation of cells and particles. *Chem Soc Rev* 36:492–506.
33. Wu M, et al. (2017) Acoustic separation of nanoparticles in continuous flow. *Adv Funct Mater* 27:1606039.
34. Lee K, Shao H, Weissleder R, Lee H (2015) Acoustic purification of extracellular microvesicles. *ACS Nano* 9:2321–2327.
35. Helwa I, et al. (2017) A comparative study of serum exosome isolation using differential ultracentrifugation and three commercial reagents. *PLoS One* 12:e0170628.
36. Petersson F, Nilsson A, Holm C, Jönsson H, Laurell T (2005) Continuous separation of lipid particles from erythrocytes by means of laminar flow and acoustic standing wave forces. *Lab Chip* 5:20–22.
37. Doss JF, et al. (2015) A comprehensive joint analysis of the long and short RNA transcriptomes of human erythrocytes. *BMC Genomics* 16:952.
38. Patrick DM, et al. (2010) Defective erythroid differentiation in miR-451 mutant mice mediated by 14-3-3zeta. *Genes Dev* 24:1614–1619.
39. Dore LC, et al. (2008) A GATA-1-regulated microRNA locus essential for erythropoiesis. *Proc Natl Acad Sci USA* 105:3333–3338.
40. Fu YF, et al. (2009) Mir-144 selectively regulates embryonic α-hemoglobin synthesis during primitive erythropoiesis. *Blood* 113:1340–1349.
41. György B, et al. (2011) Membrane vesicles, current state-of-the-art: Emerging role of extracellular vesicles. *Cell Mol Life Sci* 68:2667–2688.
42. Yamashita T, Takahashi Y, Nishikawa M, Takakura Y (2016) Effect of exosome isolation methods on physicochemical properties of exosomes and clearance of exosomes from the blood circulation. *Eur J Pharm Biopharm* 98:1–8.
43. Gopala KG, Anwar AA, Ahmad A (1990) Absorption of ultrasound in human blood. *Le J Phys, Colloq* 51:C2-311–C2-314.
44. Carter A (2011) Platelet proteomics principles, analysis, and applications. *J Am Soc Mass Spectrom* 23:430.
45. Dukhin AS, Goetz PJ, van de Ven TG (2006) Ultrasonic characterization of proteins and blood cells. *Colloids Surf B Biointerfaces* 53:121–126.
46. Augustsson P, Karlsen JT, Su HW, Bruus H, Voldman J (2016) Iso-acoustic focusing of cells for size-insensitive acousto-mechanical phenotyping. *Nat Commun* 7:11556.
47. Fadhel MN, Berndl ES, Strohm EM, Kolios MC (2015) High-frequency acoustic impedance imaging of cancer cells. *Ultrasound Med Biol* 41:2700–2713.
48. Maharjan S (2017) Lipoprotein Metabolism. Available at biochemistrymolecularbiology.blogspot.com/2015/05/lipoprotein-metabolism.html. Accessed August 17, 2017.

Supporting Information

Wu et al. 10.1073/pnas.1709210114

SI Theory and Mechanism

The integrated acoustofluidic device (Fig. 1*B*) consists of a lithium niobate ($LiNbO_3$) substrate, two pairs of IDTs, and a polydimethylsiloxane (PDMS) microchannel. The fabrication process for these devices is similar to that described in our previous work (29, 30). In summary, IDTs designed for driving frequencies of ∼20 MHz and ∼40 MHz were deposited on the $LiNbO_3$ substrate using photolithography and lift-off processes, and the PDMS microchannel was bonded onto the $LiNbO_3$ substrate in between the IDTs. The channel included the following ports: a specimen inlet for whole blood, three inlets for buffer solution as sheath flows, an outlet for blood cells, an outlet for subgroups of EVs other than exosomes, and an outlet for purified exosomes. In addition to the inlet ports for blood samples and sheath flow and outlet ports for separated components, the PDMS microchannel also contains a prefiltration pillar array at the blood sample inlet that aids in preventing blood cells from aggregating. Our device used a taSSAW described in our previous work (29, 30), where the IDTs and the PDMS microchannel were aligned at optimal angles for the desired application. In this work, those angles were 5° and 15° for the cell-removal module and the exosome-isolation module, respectively. General considerations for the design of optimal tilting angles were described elsewhere (29, 30, 33).

Particles are subjected to an acoustic radiation force (F_r) generated by the SAW field, as described by Eqs. **S1** and **S2**:

$$F_r = -\left(\frac{\pi p_0^2 V_p \beta_f}{2\lambda}\right)\phi(\beta,\rho)\sin(2kx), \qquad \textbf{[S1]}$$

$$\phi(\beta,\rho) = \frac{5\rho_p - 2\rho_f}{2\rho_p + \rho_f} - \frac{\beta_p}{\beta_f}. \qquad \textbf{[S2]}$$

In these equations, p_0, V_p, λ, k, x, ρ_p, ρ_f, β_p, and β_f represent acoustic pressure, volume of the particle, wavelength, wave number, distance from a pressure node, density of the particle, density of the fluid, compressibility of the particle, and compressibility of the fluid, respectively. Eq. **S2** is the expression for the acoustic contrast factor Φ, which determines whether each particle moves toward pressure nodes or antinodes in the SAW field. For cells and vesicles, the acoustic contrast factor is positive, indicating that they tend to move toward the pressure node.

As particles move toward the pressure nodes because of the acoustic radiation force, their movement is impeded by the Stokes drag force (F_d):

$$F_d = -6\pi\eta R_p(u_p - u_f), \qquad \textbf{[S3]}$$

where η, R_p, u_p, and u_f are viscosity of the fluid, radius of the particle, velocity of the particle, and velocity of the fluid, respectively.

The drag force is proportional to the radius of particles or cells and the acoustic radiation force is proportional to the volume. Thus, the acoustic radiation force dominates over the drag force for larger particles, which causes the particle stream to migrate toward the nodes. Conversely, the drag force cancels a significant part of acoustic radiation force out for smaller particles, resulting in little lateral displacement. By adjusting the input power, the cutoff particle diameter can be adjusted, giving our device the flexibility to be used in a wide variety of applications.

SI Simulation Assays for Isolating Nonexosomal Particles and Soluble Proteins from Exosomes

Our acoustofluidic method can separate particles not only based on size difference but also based on differences in other physical properties such as acoustic contrast factors (Table S1 and Fig. S7). Since most particles and biomolecules such as proteins aggregates and nonexosomal particles in the biological fluids have either different size or different acoustic contrast factors from exosomes (Table S1), we should be able, using solely acoustic methods, to remove most of the contaminants from exosomes. In Table S1, we provide data on the size, acoustic contrast factor, and other physical properties of nonexosomal particles and proteins (i.e., potential contaminants) such as high-density lipoproteins (HDLs), low-density lipoproteins (LDLs), intermediate-density lipoproteins (IDLs), very-low-density lipoprotein (VLDL), and chylomicrons (43–48). Among these potential contaminants, LDLs, IDLs, VLDL, and chylomicrons all have negative acoustic contrast factors. Since exosomes have a positive acoustic contrast factor, they can be easily isolated from these nonexosomal particles and proteins. More specifically, exosomes (positive acoustic contrast factors) tend to move toward pressure nodes, while these four particles (negative acoustic contrast factors) tend to move toward antipressure nodes. Although the HDLs have a positive contrast factor, just like exosomes, their large size difference from exosomes (5–12 nm vs. 30–150 nm) makes them easily separable.

We have developed a simulation code that can predict particle trajectory in the acoustic field and fluidic flow, and our simulation results match well with our experimental results (29). With our code, we conducted an additional simulation which predicts that based on the difference in acoustic contrast factor, exosomes can be isolated from other nonexosomal particles and proteins such as LDLs, IDLs, VLDL, and chylomicrons that have similar size but a negative acoustic contrast factor (shown in Fig. S7*B*). Our simulation results also predict that based on the size difference, exosomes can be further purified by removing nonexosomal particles and proteins (such as HDLs) that are smaller than exosomes in size, as shown in Fig. S7*C*.

SI Device Fabrication

The substrate to generate acoustic waves was *Y*+128° *X*-propagation $LiNbO_3$. The IDTs were fabricated using standard photolithography processes. First, a layer of SPR3012 photoresist (MicroChem Corp.) was spin-coated onto the substrate, followed by UV exposure using MA/BA6 mask aligner (SUSS MicroTec). Then, the unwanted photoresist was removed using CD26 developing solution (MicroChem Corp.). A metal double layer (Cr/Au, 50 Å/500 Å) was subsequently deposited with an e-beam evaporator (Semicore Corp.). The IDTs, with electrode widths of 50 and 25 μm, were formed on the $LiNbO_3$ substrate by a lift-off process using PRS3000 resist stripper (VWR). A PDMS microchannel with a height of 100 μm and a width of 800 μm was fabricated by standard soft lithography using an SU-8 photoresist (MicroChem). The Sylgard 184 Silicone Elastomer Curing Agent and Base (Dow Corning) were mixed at a 1:10 weight ratio, and then cast on top of the silicon mold and cured at 65 °C for 30 min. A 0.75-mm Harris Uni-Core biopsy punch (World Precision Instrument) was used to drill holes in the PDMS channel to form three inlets and two outlets. Finally, the PDMS microchannel and the $LiNbO_3$ substrate were placed in an oxygen plasma cleaner (PDC001, Harrick Plasma) for 3 min, bonded together, and cured overnight.

SI Experimental Setup

Polystyrene particles of diameter 110 nm, 970 nm, and 5 μm were purchased from Bangs Laboratory. Human whole blood was purchased from Zen-Bio, Inc., which was collected and shipped on the same day in 10-mL EDTA-coated vacutainer blood tubes. Upon arrival, the blood was stored at 4 °C before being used in the experiments. The integrated acoustofluidic platform was placed on the stage of an upright microscope (BX51WI, Olympus) with a Peltier cooling system (TEC1-12730, Hebei IT) during the separation experiment. The temperature of the Peltier cooling system was adjusted via a variable dc power supply (TP1505D, Tekpower). A CCD camera (CoolSNAP HQ2, Photometrics) recorded the separation process, and the data were analyzed with ImageJ (NIH). The sample flow and sheath fluid were individually controlled by syringe pumps (neMESYS, CETONI GmbH). The microfluidic device and syringe pumps were connected by polythene tubings (Smith Medical International) of inner diameter 0.28 mm. Before each experiment, pure ethanol was flushed through the whole microfluidic channel to remove air bubbles. Separated EVs were collected in 1.5-mL centrifuge tubes. The acoustic waves were generated by applying an rf to the IDTs on the $LiNbO_3$ substrate. The rf signal was generated by a function generator (E4422B, Agilent), and then an amplifier (100A250A, Amplifier Research) was used to provide the boost of voltage. The input power was measured by an oscilloscope (DPO4104, Tektronix). The size distribution and concentration of the isolated samples were tested with Zetasizer Nano (Malvern) and an NTA (Nanosight LM10, Malvern) system.

SI Characterization of Exosomes

Western Blot. Isolated exosomes, vesicle wastes, cell wastes, and blood samples were processed. The whole blood sample was diluted 10 times for gel electrophoresis. Before Western blot experiments, blood cells were removed by centrifugation. The samples were lysed in Pierce Cell Lysis Buffer (Thermo Fisher Scientific) with Halt Protease Inhibitor Cocktail (Thermo Fisher Scientific) mixture. Lysates were separated by SDS/PAGE and transferred to a polyvinylidene fluoride membrane (Bio-Rad). The membranes were incubated separately with mouse anti-CD63 (sc-5275, 1 μg/mL, Santa Cruz), mouse anti-HSP90 (ab13492, 1 μg/mL, Abcam), rabbit anti-TSG101 (ab30871, 1 μg/mL, Abcam), rat anti-HSC70 (ab19136, 1 μg/mL, Abcam), followed by appropriate HRP secondary antibody incubation including goat anti-mouse IgG (ab97040, 0.05 μg/mL, Abcam), goat anti-rabbit IgG (ab97080, 0.05 μg/mL, Abcam), and goat anti-rat IgG (ab7097, 0.05 μg/mL, Abcam). Finally, a Bio-Rad ChemiDoc XRS+ system was used for characterization of protein expression levels.

Electron Microscopy. For SEM imaging, isolated EVs were filtered through a membrane to remove the PBS buffer. This ensured that EVs were attached to the membrane. After washing three times with serial concentrations of ethanol (50, 70, 80, 90, 95, and 100%) for dehydration, the isolated EVs were sputtered with a thin layer of gold to increase sample conductivity and prepare for SEM imaging. For TEM imaging, the isolated exosome sample was mixed with paraformaldehyde with the final concentration of 4% wt/vol. After incubating at room temperature for 20 min, a 100-μl drop of isolated exosome sample was placed on a sheet of Parafilm (VWR). A 300-mesh copper grid support film (Electron Microscopy Sciences) was placed on the drop (membrane side down) to allow the membranes to adsorb for 20 min. Then, the grid was transferred to a 100-μl drop of distilled water for 2 min. This process was repeated three times. The grid was then transferred to a 100-μl drop of uranyl–acetate solution for negative staining for 10 min. Finally, the grid was washed again using distilled water and left to air dry at room temperature. The sample was then observed under electron microscope.

qPCR Measurement of mRNA Genes. Total RNA was extracted using QIAzol (Qiagen) from samples of human blood, cell waste, vesicle waste, and isolated exosomes. cDNA was synthesized using High-Capacity RT Kit (Thermo Fisher). Then, 10-fold diluted cDNA was used as a template in SYBR Green-based qPCR reaction in ViiA 7 qPCR instrument (Thermo Fisher). mRNA gene-specific primers were synthesized by Integrated DNA technologies. Primer sequences are listed below. The Ct values of individual mRNA were normalized by GAPDH.

qPCR primer sequence table:

FTL:

Forward: AGGCCCTTTTGGATCTTCAT

Reverse: CAGGTGGTCACCCATCTTCT

GYPA:

Forward: CAGAGACAAGTGATCAATGAG

Reverse: AATTGTACAACTTAGGCAGG

TFRC:

Forward: AAGATTCAGGTCAAAGACAG

Reverse: CTTACTATACGCCACATAACC

SLC25A37:

Forward: GGTAATGAATCCAGCAGAAG

Reverse: AGGAACTCATAGGTGATGAAG

qPCR Measurement of Mature miRNA. Total RNA was extracted using QIAzol (Qiagen) from human blood input and isolated exosomes. cDNA was synthesized using miScript RT Kit (Qiagen). Mature miRNA-specific primers were purchased from Qiagen and used in SYBR Green-based qPCR reaction in ViiA 7 qPCR instrument (Thermo Fisher). The Ct values of individual miRNA were normalized by spike-in cel miR-39–3p.

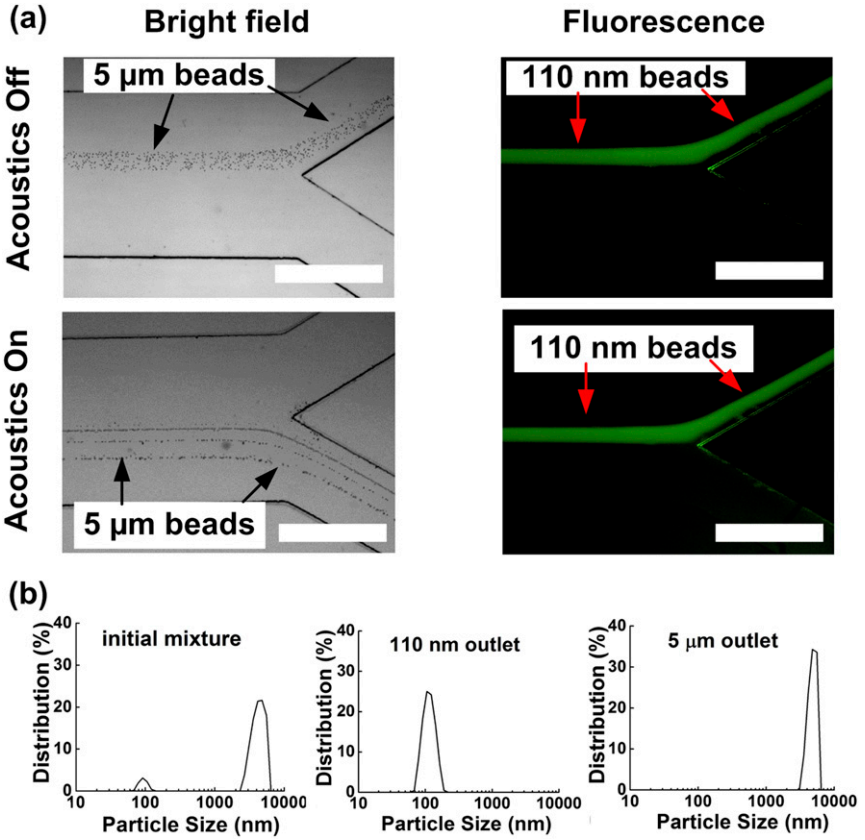

Fig. S1. Validation of the cell-removal module with polystyrene particles. (*A*) Polystyrene particles with diameters of 5 μm (not labeled) and 110 nm (labeled with Dragon Green fluorescent dye) are mixed and processed using the cell-removal module. (Scale bar: 500 μm.) (*B*) Particle size distribution of initial mixture and collected samples was measured by DLS. The initial mixture had two distinct size-distribution peaks; in contrast, the processed sample exhibited only one peak for both samples collected from the top and bottom outlets.

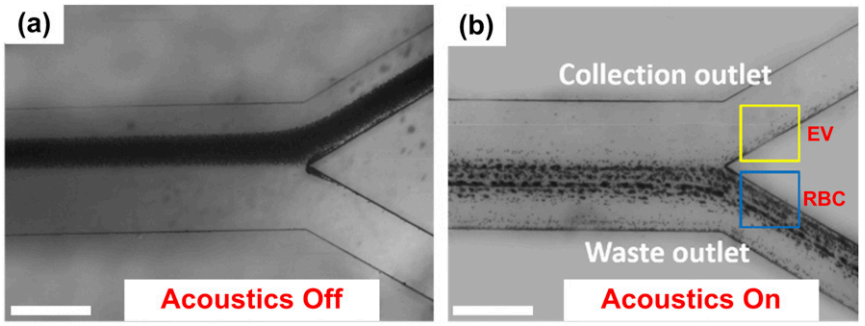

Fig. S2. Isolation of EVs from whole blood using the cell-removal module. The images at outlet region when acoustic waves are (*A*) off and (*B*) on. Blood cells are pushed to bottom outlets when the acoustic field is on. White stripe in the figure indicates the centerline location of the CCD image sensor. (Scale bar: 500 μm.)

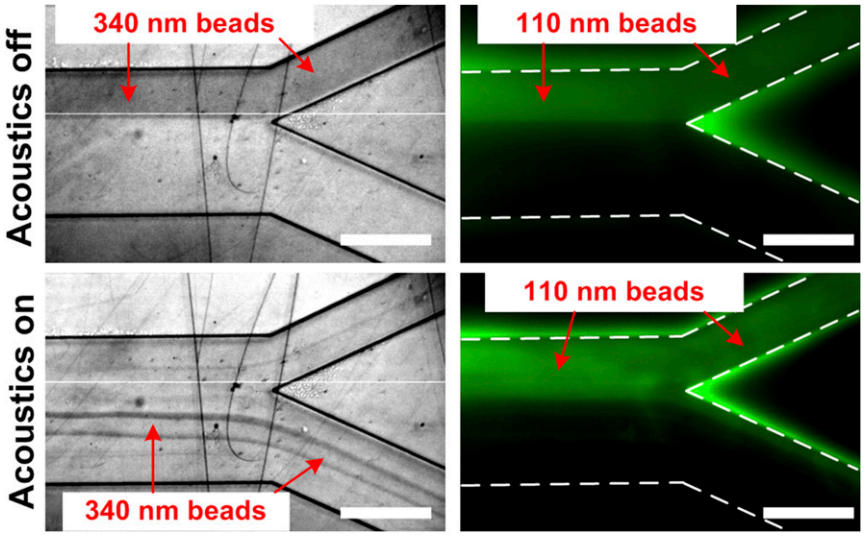

Fig. S3. Separation of 340- and 110-nm particles using the exosome isolation module. White stripe in the two left panels indicates the centerline location of the CCD image sensor. (Scale bar: 500 μm.)

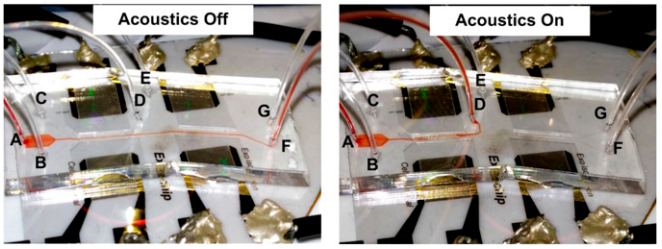

Fig. S4. Isolation of EV subgroups from whole blood using the integrated acoustofluidic device. The inlets and outlets are (*A*) whole-blood inlet; (*B*, C, and *E*) sheath flow inlets; (*D*) cell waste outlet; (*F*) exosome outlet; (*G*) vesicle waste outlet. The blood cells are deflected to outlet D; EV subgroups other than exosomes are pushed to G when the acoustic field is on. Purified exosomes are collected from outlet F.

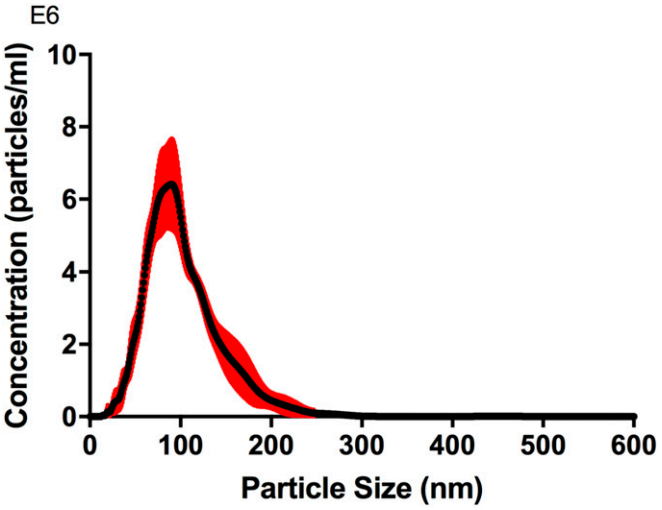

Fig. S5. Size distribution of isolated human plasma exosomes using the Opti-Prep-based gradient ultracentrifugation technique (16). The mean size of the exosomes was 104.15 ± 7.60 (n = 3), which was slightly larger than that of exosomes isolated from human blood using the acoustofluidic device.

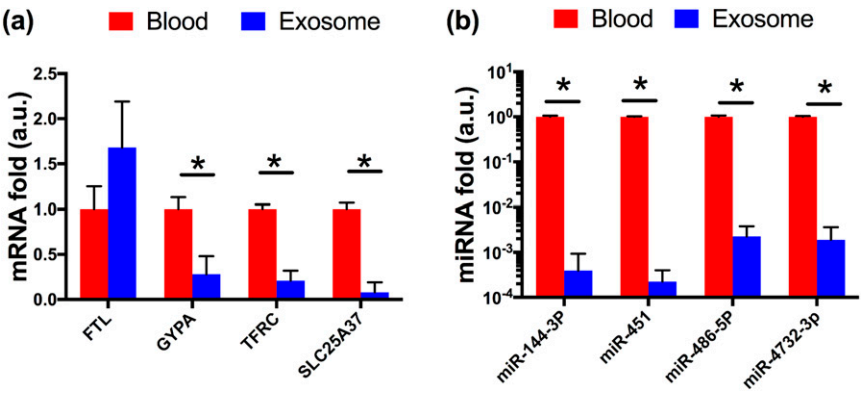

Fig. S6. Relative levels of mRNA and miRNA transcripts in human blood versus isolated exosomes using OptiPrep gradient ultracentrifugation. Fold changes of individual mRNAs (*A*) and miRNAs (*B*) in human blood and isolated exosomes were quantified by qPCR. Results were derived from three different blood samples and analyzed using a one-way ANOVA post hoc test. The asterisk indicates statistical significance with adjusted P value < 0.05.

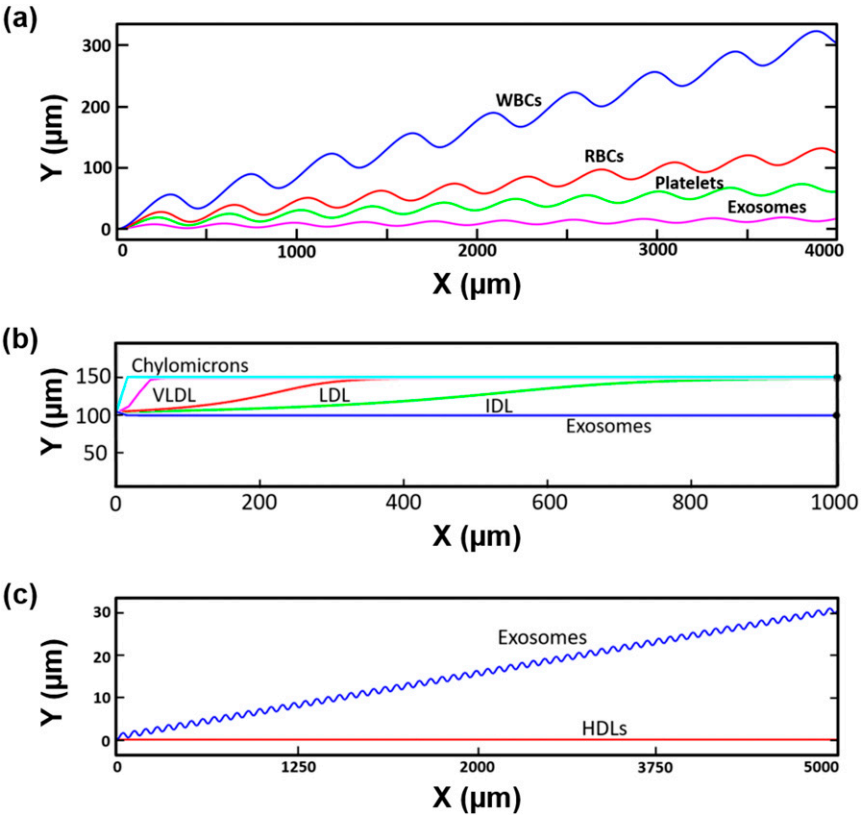

Fig. S7. Simulation results showing that by using our acoustic methods: (*A*) exosome can be first isolated from blood cells and other EVs based on size difference; (*B*) isolated exosomes can then be purified based on the difference in acoustic contrast factor by isolating exosomes from nonexosomal particles and proteins that have negative acoustic contrast factor, such as LDLs, IDLs, VLDL, and chylomicrons; (*C*) exosomes can be further purified based on the size difference by isolating exosomes from particles smaller than exosomes such as HDLs.

Table S1. Physical parameters of blood cells, exosomes, and other nonexosomal particles and proteins that are often present in biological fluids (43–48)

Blood components	Diameter, nm	Density, kg/m^3	Lipid percentile	Speed of sound, m/s	Compressibility, 1/Pa	Acoustic contrast factor
RBCs (43, 44)	6,200–8,200	1,090–1,100	—	1,689.50	3.2×10^{-10}	0.3966
WBCs (45–47)	6,000–15,000	1,060–1,090	—	1,609.30	3.59×10^{-10}	0.2939
PLTs (44)	2,000–5,000	1,040–1,060	—	1619.05	3.3×10^{-10}	0.2622
Exosomes (34)	30–150	∼1,130	—	1,590.11	3.50×10^{-10}	0.3616
HDLs (48)	5–12	1,063–1,210	45–60%			
LDLs (48)	18–25	1,019–1,063	78%	1,325.65	5.49×10^{-10}	−0.1463
IDLs (48)	25–35	1,006–1,019	83%	1,362.29	5.32×10^{-10}	−0.1406
VLDLs (48)	30–80	950–1,006	92%	1,422.04	5.14×10^{-10}	−0.1367
Chylomicrons (48)	100–1,000	<950	98%	1,452.63	4.99×10^{-10}	−0.1335

HDLs, LDLs, IDLs, VLDL, and chylomicrons are considered the most common nonexosomal particles and proteins.